

# Muon transfer from muonic hydrogen to atomic oxygen and nitrogen

Anh-Thu Le\* and C. D. Lin

Department of Physics, Cardwell Hall, Kansas State University, Manhattan, Kansas 66506, USA

(Received 15 October 2004; published 17 February 2005)

The results of diabatic hyperspherical close-coupling calculations are presented for the charge exchange of a negative muon from muonic hydrogen to oxygen and nitrogen for collision energies from  $10^{-3}$  to  $10^3$  eV. It is shown that converged results can be obtained using a much smaller number of channels than in the traditional adiabatic approach. For the energy range below 10 eV our results for nitrogen are in good agreements with the available experimental data and the recent calculations within hyperspherical elliptic coordinates. However, discrepancies were found in the case of oxygen, where a  $p$ -wave shape resonance is shown to contribute significantly to the cross sections. We show that for oxygen the  $p$ -wave resonance extends to a large volume and is sensitive to the many-body effect. Calculations including outer screening of the oxygen atom have been performed to illustrate the importance of this effect.

DOI: 10.1103/PhysRevA.71.022507

PACS number(s): 36.10.Dr, 34.70.+e, 31.15.Ja

## I. INTRODUCTION

Muon transfer between muonic hydrogen and other atoms has been investigated for over 40 years, both experimentally and theoretically (see, for example, [1] and references therein), in the framework of muon-catalyzed fusion, where even a small amount of high- $Z$  atom contamination can significantly affect the fusion reaction by preventing the muon from continuing the chain reaction. It is therefore not surprising that a good number of experiments have been carried out to study muon transfer to high- $Z$  atoms [2–5]. Whereas early interest in this problem was related to the muon-catalyzed fusion program, recent interest is more related to metrology and tests for quantum electrodynamic theories (see, for examples, Refs. [6–8]).

On the theoretical side, these three-body reactions involving heavy-particle transfer continue to be challenging problems. The large charge of the nuclei leads to a strong polarization of the muonic hydrogen in the initial channel and strong Coulomb repulsion in the final channels. Furthermore, the number of open channels even at zero collision energy increases quickly with  $Z$ . Therefore it is not surprising that until recently there had been no quantum dynamical calculations for these systems.

The first theoretical work for muon capture was done in 1963 by Gershtein [9], who gave a systematic investigation within the Landau-Zener model. The first quantum dynamical calculations involving high-charge atoms were done only recently by Sultanov and Adhikari [10], who solved two-state integro-differential equations within the Faddeev equation formalism for carbon and oxygen. In a series of papers, Dupays *et al.* [11,12] and Dupays [13] quite recently performed calculations using hyperspherical elliptic coordinates. They included a large number of channels and found reasonably good agreement with experiments for nitrogen, oxygen, and neon colliding with muonic protium and deuterium atoms.

Since the muon-transfer reaction in collisions between muonic hydrogen and atoms occurs at very small internuclear distances [9], until now most of the theoretical models consider the atom as a bare nucleus. Helium is an exception [14]. The importance of resonant effects at epithermal energies was first noticed by Kravtsov *et al.* in the elastic cross sections [15]. In a semiclassical two-state model calculation Savichev and Blümel [16] showed that in  $p\mu\text{-O}^{8+}$  collisions, the charge-transfer rate would have a dominant peak at epithermal energies due to the resonance effect. Quite recently, Romanov [17] showed the effect of screening on the resonances in  $p\mu\text{-Ne}$  collisions, using a Jacobi coordinate coupled-channel method.

In this paper we investigate the muon transfer in  $p\mu(1s)$  colliding with atomic oxygen and nitrogen for collision energies from  $10^{-3}$  to  $10^3$  eV using the recently developed diabatic hyperspherical close-coupling (HSCC) method and the truncation of channels technique [18–20]. The idea of channel truncation is very simple. Once the molecular basis set is diabaticized, the channels that couple weakly with the entrance channel can be removed from the close-coupling calculations without significant loss of accuracy. In this paper, we show that for collision energies below 10 eV, only five channels are needed to get converged results. This should be compared to the use of 88 channels in the calculations by Dupays *et al.* [11,12] and Dupays [13] for the same systems. We also show that using this approach, the calculations for higher partial waves do not pose any difficulties so one can easily perform calculations for collision energies up to 1 keV or higher, still with a relatively small number of channels.

The paper is organized as follows. In Sec. II we briefly describe the HSCC method and the diabaticization technique. The results are presented in Sec. III. The last section contains a summary and conclusion.

All the energies are given in the center-of-mass frame and atomic units are used unless otherwise indicated.

## II. THEORETICAL METHOD

The HSCC method has been used previously to study charge transfer in ion-atom collisions [21]. We refer the

\*Electronic address: atle@phys.ksu.edu

reader to Liu *et al.* [21] for details on the method and Le *et al.* [19] and references therein for more recent results on ion-atom collisions. The method has also been applied to other three-body collisions involving different combinations of masses such as antiproton-H [18] and positron-alkali-metal collisions [22]. The diabatization and elimination of weak channels were introduced by Hesse *et al.* [18] and have been applied by Le *et al.* to He<sup>2+</sup>-H [19] and by Lee *et al.* to O<sup>8+</sup>-H and Ar<sup>8+</sup>-H [20]. Here we summarize only the essentials of the method.

The three-body problem, say for muon transfer in  $p\mu\text{-O}^{8+}$ , is solved in mass-weighted hyperspherical coordinates. In the ‘‘molecular’’ frame, the first Jacobi vector  $\boldsymbol{\rho}_1$  is chosen to be the vector from O<sup>8+</sup> to the proton, with reduced mass  $\mu_1$ ; and the second Jacobi vector  $\boldsymbol{\rho}_2$  goes from the center of mass of O<sup>8+</sup> and the proton to the muon, with reduced mass  $\mu_2$ . The hyperradius  $R$  and hyperangle  $\phi$  are defined as

$$R = \sqrt{\frac{\mu_1}{\mu} \rho_1^2 + \frac{\mu_2}{\mu} \rho_2^2}, \quad (1)$$

$$\tan \phi = \sqrt{\frac{\mu_2 \rho_2}{\mu_1 \rho_1}}, \quad (2)$$

where  $\mu$  is arbitrary. In this paper we chose  $\mu = \sqrt{\mu_1 \mu_2}$ . We further define an angle  $\theta$  as the angle between the two Jacobi vectors. The two angles  $\{\phi, \theta\}$ , to be denoted as  $\Omega$ , describe the internal motion of the particles. For describing the rotation of the whole system we use three Euler angles  $\hat{\omega} = \{\omega_1, \omega_2, \omega_3\}$  of the body-fixed frame axes with respect to the space-fixed frame.

The HSCC treats the hyperradius  $R$  as a slow variable, similarly to the way the Born-Oppenheimer (BO) approximation treats the internuclear distance. Thus we first solve the adiabatic equation with hyperradius  $R$  fixed to obtain adiabatic channel functions  $\Phi_{\nu I}^A(R; \Omega)$  and adiabatic potential energies  $U_{\nu I}^A(R)$ . Here  $\nu$  is the channel index, and  $I$  is the absolute value of the projection of total angular momentum  $\mathbf{J}$  along the body-fixed  $z'$  axis, taken to be the axis between O<sup>8+</sup> and the proton. The superscript ‘‘A’’ designates the channel functions as adiabatic. We solve this equation by using  $B$ -spline basis functions. Typically about 160 and 80 grid points are used for  $\phi$  and  $\theta$ , respectively. Special care was taken so that more grid points were distributed near the singularities of the Coulomb interactions among the three particles.

In the next step of the adiabatic HSCC, similarly to the standard BO approach, we solve the Schrödinger equation by expanding the wave function in the adiabatic basis,

$$\Psi(R, \Omega, \hat{\omega}) = \sum_{\nu} \sum_I F_{\nu I}(R) \Phi_{\nu I}^A(R; \Omega) \tilde{D}_{IM}^J(\hat{\omega}). \quad (3)$$

In this equation,  $\tilde{D}$  is the normalized and symmetrized rotation function, and  $M_J$  is the projection of angular momentum  $\mathbf{J}$  along the space-fixed  $z$  axis.

To be able to eliminate the weak channels from the subsequent close-coupling calculations, we first transform from the adiabatic basis set to a diabatic one. Formally, adiabatic and diabatic representations are related by a unitary transformation, written in matrix form as follows:

$$\Phi^D = C\Phi^A, \quad (4)$$

where  $\Phi^A$  and  $\Phi^D$  are the adiabatic and diabatic channel functions, respectively, and  $C$  is a unitary matrix. Note that the diabatic representation is not defined uniquely and depends on how the transformation matrix  $C$  is determined. For our purpose, we define  $C$  in such a way that  $\Phi^D$  is as least sensitive as possible to the variation of hyperradius  $R$  within the subspace spanned by  $\Phi^A$ . In other words, we require

$$\Delta\Phi^D(R) \equiv \Phi^D(R + \Delta R) - \Phi^D(R) = 0, \quad (5)$$

or more explicitly (for simplicity, we omit the  $I$  index in the following equations),

$$\sum_{\nu} [C_{\mu\nu}(R + \Delta R) \Phi_{\nu}^A(R + \Delta R) - C_{\mu\nu}(R) \Phi_{\nu}^A(R)] = 0. \quad (6)$$

Multiplying both sides of the above equation by  $\Phi_{\lambda}^A(R + \Delta R)$  and integrating over the angles, we get

$$C_{\mu\lambda}(R + \Delta R) = \sum_{\nu} C_{\mu\nu}(R) \langle \Phi_{\nu}^A(R) | \Phi_{\lambda}^A(R + \Delta R) \rangle. \quad (7)$$

In practice, in order to diabatize the sharp avoided crossings we limit the summation in the above equation to a few channels which have the largest overlaps. More precisely, we choose to include in the summation in Eq. (7) only those channels  $\nu$  whose overlaps at two neighboring points satisfy

$$|\langle \Phi_{\nu}^A(R + \Delta R) | \Phi_{\lambda}^A(R) \rangle| > \alpha, \quad (8)$$

where  $\alpha$  is typically chosen equal to 0.2. The diabatization should be started from a large enough distance where one can choose the initial condition for  $C$  to be the identity matrix. Using Eqs. (7) and (8), the transformation matrix  $C$  is then propagated down to  $R=0$ . Once the diabatic basis is obtained, further implementation of the diabatic HSCC approach is straightforward with the adiabatic channel functions in the expansion (3) replaced by the diabatic ones. The main advantage of this procedure is that it allows us to conveniently discard channels that are weakly coupled to the main channels. The main channels are defined to be those that couple strongly with the entrance channel and among themselves. Moreover, since only the sharp avoided crossings are diabatized, our intuitive adiabatic picture of the collision dynamics, based on the important broad avoided crossings, is still valid.

In the last step we solve the coupled hyperradial equations using a combination of the  $R$ -matrix propagation [23] and slow or smooth variable discretization (SVD) [24] techniques. The hyperradius range is divided into sectors and the SVD is used in each sector. The  $R$  matrix is then propagated from one sector to the next up to a large hyperradius where the solutions are matched to the known asymptotic solutions to extract the scattering matrix  $S_{ij}^J$ . The calculations are carried out for each partial wave until a converged cross section is

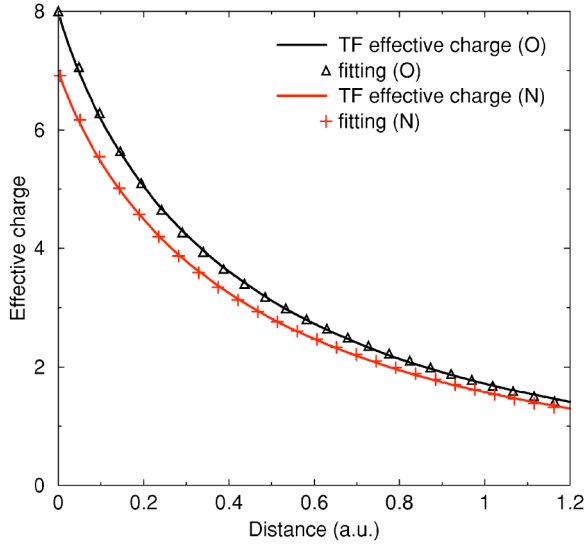


FIG. 1. (Color online) Thomas-Fermi effective charge for oxygen and nitrogen as function of the distance from the nucleus. The fittings to Eq. (12) are also shown as  $\Delta$  (oxygen) and  $+$  (nitrogen).

reached. The total cross section for transition from initial state  $i$  to final state  $j$  is given as the sum over all the partial-wave cross sections by

$$\sigma_{ij}(E) = \sum_J \sigma_{ij}^J(E) = \frac{\pi}{k_i^2} \sum_J (2J+1) P_{ij}^J(E), \quad (9)$$

where the transition probability  $P_{ij}^J(E)$  is given as  $|S_{ij}^J|^2$  and  $k_i$  is the initial momentum.

For relative collision velocity  $v$ , the muon-transfer rate is defined as

$$\lambda(E) = Nv\sigma(E). \quad (10)$$

This value is traditionally reduced (or normalized) to the atomic density of liquid hydrogen with  $N=N_H=4.25 \times 10^{22} \text{ cm}^{-3}$ . To relate to experimental data, we need to calculate the temperature-dependent rate, defined as the average value of the energy-dependent muon-transfer rate, convoluted with a Maxwellian kinetic energy distribution at a given temperature  $T$  at which the experiments have been carried out,

$$\lambda(T) = \int_0^\infty \lambda(E) \sqrt{\frac{4E}{\pi(kT)^3}} \exp(-E/kT) dE, \quad (11)$$

where  $k$  is the Boltzmann constant.

In general, the dynamics of the electron shell during the collision is a complicated problem. The simplest approximation is to assume that the electron shell remains in the ground state. The role of the electron cloud is then reduced to the screening of the electrostatic interaction between the nucleus and the muonic hydrogen. In order to investigate the effect of electron screening, we use a simple Thomas-Fermi (TF) potential [25]. The effective charges for oxygen and nitrogen are shown in Fig. 1. For computational convenience, the effective charges were fitted to an analytical function in the form

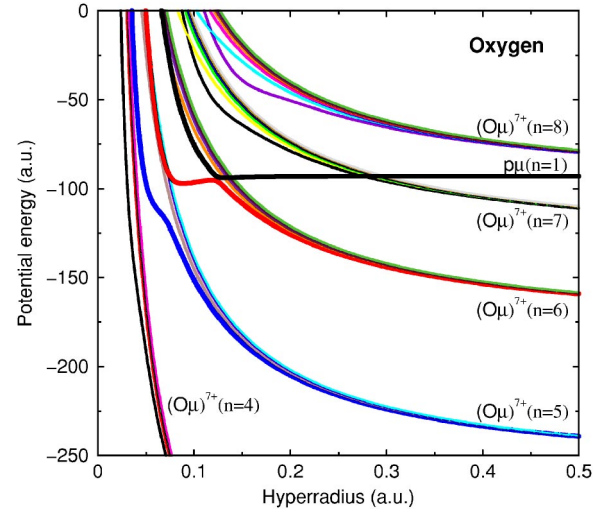


FIG. 2. (Color online)  $J=0$  diabatic potential curves for  $p\mu(1s)\text{-O}^{8+}$  up to the  $(O\mu)^{7+}(n=8)$  threshold.

$$Z_{\text{eff}} = Z_{\text{nuc}} \exp(-a_0 r) + a_1 r \exp(-a_2 r) \quad (12)$$

with  $a_0$ ,  $a_1$ , and  $a_2$  equal to 1.3628,  $-10.5135$ , 3.469 71, and 1.318 44,  $-8.78476$ , 3.389 27 for oxygen and nitrogen, respectively. The fittings were done up to  $r=1.2$  a.u., which corresponds to hyperradius  $R \approx 2$  a.u., where the matching to the asymptotic solutions is performed. The fittings for oxygen and nitrogen are also shown in Fig. 1.

### III. RESULTS AND DISCUSSION

The  $J=0$  diabatic potential curves for the  $p\mu\text{-O}^{8+}$  system are presented in Fig. 2, up to the  $(O\mu)^{7+}(n=8)$  threshold. The curves are labeled in accordance with their asymptotic limits. We note, in particular, the broad avoided crossings between the entrance channel (black thick curve) and the lowest channels from the  $(O\mu)^{7+}(n=5)$  manifold (blue thick curve) and the  $(O\mu)^{7+}(n=6)$  manifold (red thick curve) just below and above  $R=0.1$  a.u., respectively. As we will see, these avoided crossings are the most important in determining the charge-transfer dynamics.

First we compare in Fig. 3 our results for the muon-capture probability for the  $s$  wave with the recent results by Dupays *et al.* [11], who used 88 channels in their close-coupling calculations. Our three-channel basis includes only the lowest channels from  $(O\mu)^{7+}(n=5)$  and  $(O\mu)^{7+}(n=6)$  together with the entrance channel, whereas the 31-channel basis includes all the channels from  $(O\mu)^{7+}(n=4)$  up to  $(O\mu)^{7+}(n=8)$ . The agreements are very good for the whole range of energy up to 1 keV with our results lying somewhat lower than those of Dupays *et al.* for energies above about 100 eV. Note the dominant contribution from the transition to  $n=5$ , especially below about 10 eV. It should be emphasized that our three-channel calculations agree very well with the 31-channel calculations, clearly indicating the dominant importance of these three channels in the collision dynamics.

Next we examine in more detail the energy region below 10 eV. It has been noticed by Savichev and Blümel [16],

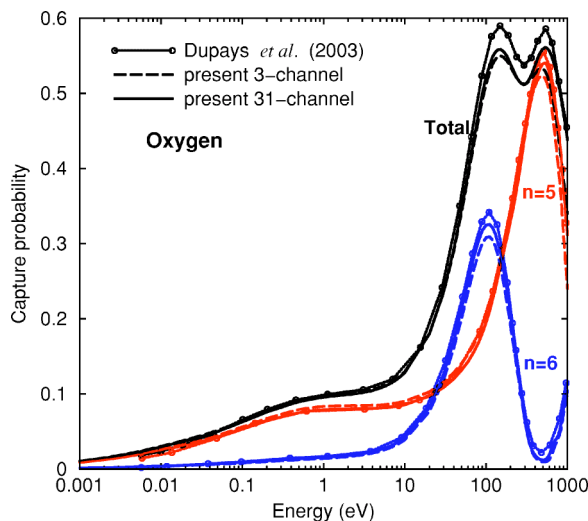


FIG. 3. (Color online) Partial and total muon-capture probability, as function of collision energy, in  $p\mu(1s)\text{-O}^{8+}$  for  $J=0$ .

Romanov [17], and Dupays *et al.* [12] that higher partial waves up to  $J=4$  can contribute significantly to the capture cross sections. Our results of five-channel calculations for the muon transfer rate are shown in Fig. 4, together with the data from 88-channel calculations by Dupays *et al.* Besides the three channels that are included in the three-channel calculations, we add the two lowest  $I=1$  channels from the  $(\text{O}\mu)^{7+}(n=5)$  and  $(\text{O}\mu)^{7+}(n=6)$  manifolds. The most prominent feature is that our  $p$ -wave resonance is much narrower and higher. The peak near 0.04 eV is about a factor of 8 higher than the corresponding value from Dupays *et al.* However, above  $E=0.3$  eV the two calculations agree quite well. For the other partial waves the two calculations are in generally good agreement. The figure also shows that at low energies the  $s$ -wave transfer rate is almost energy independent and tends to a constant value in the  $E \rightarrow 0$  limit, in accordance with the Wigner threshold law (see, for example, the review paper by Sadeghpour *et al.* [26]). For other partial

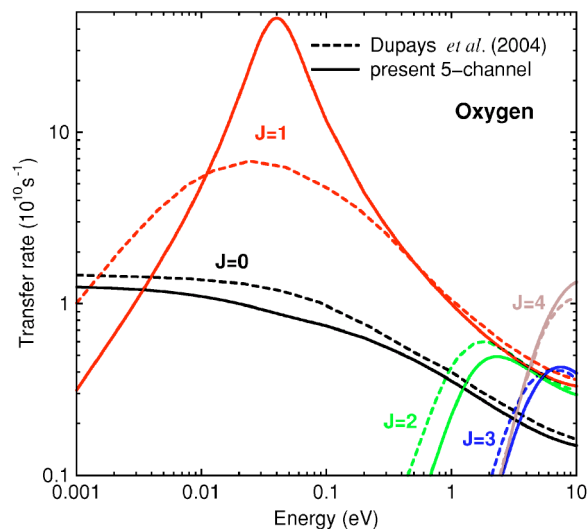


FIG. 4. (Color online) Partial-wave muon-transfer rate in  $p\mu(1s)\text{-O}^{8+}$  as function of collision energy below 10 eV.

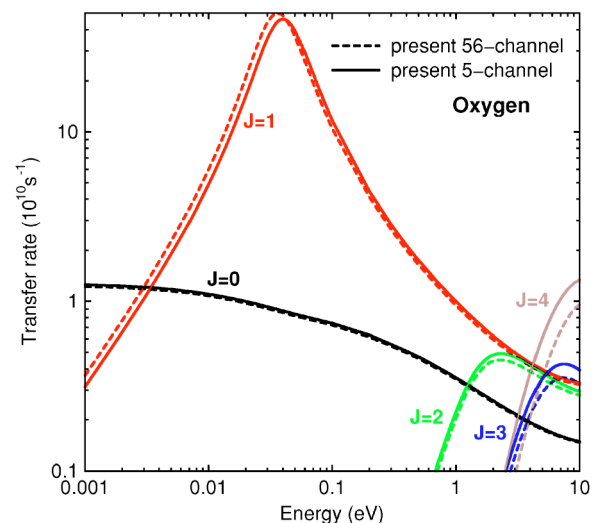


FIG. 5. (Color online) Comparison between 56-channel and five-channel calculations for  $p\mu(1s)\text{-O}^{8+}$  at low energies.

waves, the barrier in the potential curve prevents the collision system from penetrating into the reaction region, and as a result, the corresponding transition rates drop quickly.

To check the convergence, we performed calculations including up to 56 channels from the  $(\text{O}\mu)^{7+}(n=4)$  up to  $(\text{O}\mu)^{7+}(n=8)$  threshold, with 31 channels from  $I=0$ , and 25 channels from  $I=1$ . The results are presented in Fig. 5 together with the results from five-channel calculations. The comparison clearly shows that the five-channel approximation is quite adequate for the range of energy below 10 eV. Further increase in the number of channels, including channels with higher  $I$ , does not change the results significantly. Furthermore, we performed calculations for  $p$  waves with 56 *adiabatic* channel functions. The results agree very well with the 56-channel *diabatic* calculations and are indistinguishable on the scale shown in Fig. 5. We also changed the matching radius to ensure that stable results were reached.

In order to understand the origin of the discrepancy between our results and that of Dupays *et al.* we used different angular grid distributions in solving the adiabatic equation to get the adiabatic potential curves with different levels of accuracy. In general, our method achieves about 7–8 digits of accuracy for the entrance channel. Nevertheless, we found that small variations in the accuracy of the potential energies did not lead to any significant changes in the transfer rate. Furthermore, we have estimated the centrifugal barrier in the entrance channel for the  $p$  wave. The result is 0.100 eV as compared to 0.09 eV of Dupays *et al.* (see Table I from [12]). Note that our estimate is based on the HSCC potential energy plus the diagonal term of the nonadiabatic couplings. This somewhat overestimates the barrier height (see, for example, [27]). One can also use a simple estimate based on the asymptotic behavior for ion-dipole interaction:

$$U_{\text{eff}}(r) = -\frac{\alpha Z^2}{2r^4} + \frac{J(J+1)}{2Mr^2}. \quad (13)$$

Here  $\alpha$  is the dipole polarizability of  $p\mu(1s)$ , equal to  $4.5r_0^3$ , with  $r_0$  being the radius of  $p\mu(1s)$ ,  $M$  is the reduced mass of

the nucleus with respect to the muonic hydrogen, and  $r$  is the nucleus- $p\mu$  distance. This gives the barrier height of 0.084 eV. The position of the maximum is at hyperradius  $R = 0.499$  a.u., as compared to the asymptotic estimate of  $R = 0.520$  a.u. As we will see below for the case of the screening potential, a small change in the barrier height and position would lead to a change in the muon-transfer rate, but the general shape of the resonance would not change. At present the origin of the discrepancy between the HSCC and hyperspherical elliptic coordinates method for  $p$ -wave resonance is not understood.

To compare with experimental data, we need to calculate the temperature-dependent rate, as defined in Eq. (11), for room temperature  $T = 300$  K, at which the experiments have been carried out [5]. Our result for the thermal muon-transfer rate is  $2.32 \times 10^{11} \text{ s}^{-1}$ , which is about three times higher than the experimental value of  $8.5 (\pm 0.2) \times 10^{10} \text{ s}^{-1}$  [5]. It should be noted that Dupays *et al.* obtained a thermal rate of  $7.77 \times 10^{10} \text{ s}^{-1}$ , in much better agreement with the experiment. The result by Sultanov and Adhikari of  $7.7 (\pm 0.5) \times 10^{10} \text{ s}^{-1}$  [10] should not be considered too seriously since they included only the  $J=0$  partial wave whereas the results of our calculations and of Dupays *et al.* both indicate that the dominant contribution comes from the  $J=1$  partial wave.

To understand the origin of the discrepancy with the experiment we first notice that the maximum of the  $p$ -wave centrifugal barrier occurs at quite a large hyperradius of about  $R = 0.5$  a.u., which corresponds to the internuclear distance of about 0.28 a.u. At that distance, the screening effect by the electrons in oxygen should generally be taken into account, as evident from the Thomas-Fermi effective charge, shown in Fig. 1. To have an estimate of the effect of screening we performed the calculation with a simple Thomas-Fermi potential, as given in Eq. (12). A simple estimate can be made based on Eq. (13). Generally, the smaller value of the effective charge due to the screening makes the dipole-ion interaction weaker, so the potential barrier is higher. Therefore, it is expected that the general effect of screening is to weaken the interaction between oxygen and muonic hydrogen and to shift the position of the resonance to higher energy. In fact, the peak of the barrier is higher by about 10% and the position of the peak is shifted to smaller hyperradius by about 5%. Comparison of the partial-wave muon-transfer rates for the screened and unscreened models is presented in Fig. 6.

The most profound effect, as one can see from the figure, is for the  $p$  wave. Consistent with what was mentioned above, the peak of the resonance is shifted to  $E = 0.11$  eV, instead of 0.04 eV as in the unscreened case. The resonance is also less sharp. The transfer rates for other partial waves are not changed significantly. With the screening effect taken into account, our result for the thermal muon-transfer rate is  $4.42 \times 10^{10} \text{ s}^{-1}$ . This is about a factor of 2 smaller than the experimental value, and a factor of 5 smaller than in the unscreened case. Note that similar sensitivity of the transfer rate due to electron screening was also found recently by Romanov for  $d$ -wave resonance in  $p\mu$ -Ne collisions [17].

It is interesting to note that our results for the  $d$  wave are consistent with those of Dupays *et al.* [12], who also found a relatively weak  $d$ -wave resonance peak at about 2 eV. This is

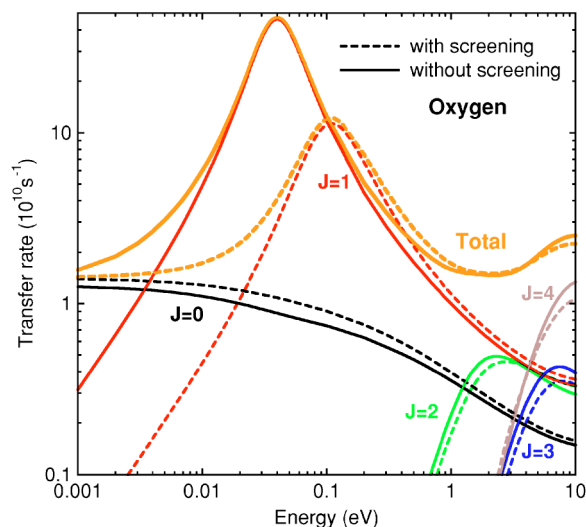


FIG. 6. (Color online) Comparison of transfer rates for the cases with and without Thomas-Fermi screening in oxygen.

in disagreement with the earlier calculations within a semiclassical two-state model by Savichev and Blümel [16] who found an intense  $d$ -wave resonance at much lower energy of about 0.2 eV. Furthermore, they argued that the existence of this intense resonance could explain the double-exponential behavior in the x-ray decay time spectra, observed in the measurements for the oxygen case [5]. Indeed, based on the two-component model of Schneuwly [28], a Monte Carlo simulation was performed to fit the double-exponential behavior and a large epithermal rate of  $3.9 \times 10^{11} \text{ s}^{-1}$  was found [5]. Our result for the “bare” interaction instead has a large contribution from  $p$ -wave resonance, peaked near  $E = 0.04$  eV. Since the  $p$ -wave resonance is sensitive to the details of the interaction potential, it is possible that a more realistic account of the interaction between oxygen and muonic hydrogen could reproduce the experimental data at thermal energies and the results of the Monte Carlo simulation for epithermal energies.

Similar to the oxygen case, we also performed the calculations for nitrogen. The results for the muon-transfer rate below 10 eV are shown in Fig. 7 together with the results from Dupays [13]. The general agreement between the two calculations is very good, with our results lying somewhat lower. Note that at and below thermal energies, mainly the  $s$  wave contributes. The  $d$ -wave resonance is quite intense with the peak shifted to a bit higher energy of about 0.9 eV, as compared to the results by Dupays. The structure near  $E = 2$  eV reported by Dupays [13] is not reproduced in our calculations. The thermal muon-transfer rate obtained with the Maxwellian distribution at room temperature is  $3.2 \times 10^{10} \text{ s}^{-1}$ . This value is in excellent agreement with the experimental value of  $3.4 (\pm 0.7) \times 10^{10} \text{ s}^{-1}$  [2]. With the screening effect taken into account the thermal muon-transfer rate is  $3.0 \times 10^{10} \text{ s}^{-1}$ . The weak effect of the screening on the muon-transfer rate, as compared to the oxygen case, can be understood, as the  $p$ -wave shape resonance is less profound and occurs at higher energies so its contribution is relatively small at thermal energies. For completeness, we show the partial-wave and total muon-transfer rates with

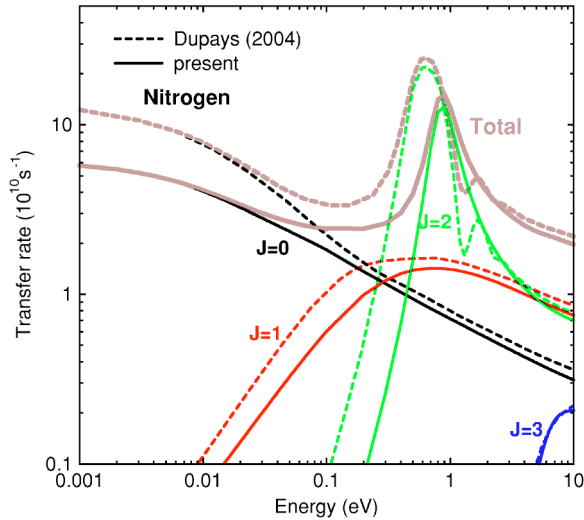


FIG. 7. (Color online) Similar to Fig. 4, but for nitrogen. Total transfer rate is also shown [lighter (brown) curves].

screening effect taken into account in Fig. 8. The values of the thermal muon-transfer rate for oxygen and nitrogen are summarized in Table I.

We next consider the higher-energy region. The simplicity of the present method allows us to calculate higher partial waves without much difficulty. In this work we extend the calculations up to a collision energy of 1 keV for both oxygen and nitrogen. To get converged results, partial waves up to  $J=30$  were calculated. For the nitrogen case, mainly  $J \leq 25$  contribute. The convergence test with respect to the number of channels for the oxygen case is shown in Fig. 9 for a few partial waves  $J=5, 10, 15, 20,$  and  $25$ . In the upper panel we compare the results from five- and seven-channel calculations. Compared to the five-channel basis, the seven-channel basis has two additional  $I=2$  lowest channels from the  $(O\mu)^{+7}(n=5)$  and  $(O\mu)^{+7}(n=6)$  manifolds. There are no visual differences between the results from the two calculations on the scale shown in the figure. This implies very weak coupling between the  $I=2$  channels and the main chan-

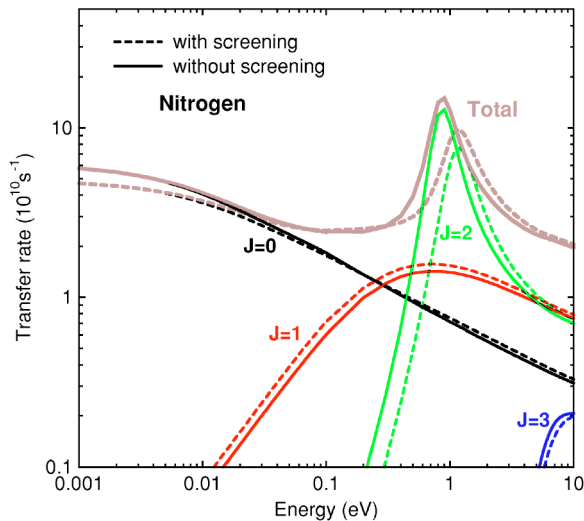


FIG. 8. (Color online) Similar to Fig. 6, but for nitrogen.

TABLE I. Total average muon-transfer rates, obtained with the Maxwellian distribution at room temperature. The bottom lines correspond to the results with screened interaction. The experimental data are taken from [2,5]; theoretical results of the hyperspherical elliptic coordinates calculations are taken from Dupays [13]. The rates are given in units of  $10^{10} \text{ s}^{-1}$ .

Atom	Present	Dupays [13]	Expt.
Oxygen	23.2	7.77	
	4.42		$8.5 \pm 0.2$
Nitrogen	3.2	5.2	
	3.0		$3.4 \pm 0.7$

nels. A similar situation has been observed in ion-atom collisions at low energies, where mainly the  $I=0, 1$  channels contribute. The lower panel compares 11-channel with 56-channel calculations. The 11-channel basis includes five  $I=0$  and five  $I=1$  lowest channels from the  $(O\mu)^{+7}(n=5)$  to  $(O\mu)^{+7}(n=9)$  manifolds together with the entrance channel. Clearly, nearly converged results can be obtained with about 11 channels even for energies up to 1 keV. In fact, inclusion of two additional channels from the  $n=4$  manifold would lead to much better agreement with the 56-channel results. Further increase in the number of channels does not change the results significantly. This figure also shows a relatively small contribution from  $J=25$ , but it would apparently be important for energies above 1 keV. We show in Fig. 10 the total muon-transfer rates for oxygen and nitrogen. Note the different behaviors for the two cases, with the rate for nitrogen increasing much faster compared to that of oxygen at collision energies below about 300 eV. The small structures in the oxygen case are due to the resonances associated with  $J=5, 6,$  and  $7$  (see also Fig. 9 for the case  $J=5$ ).

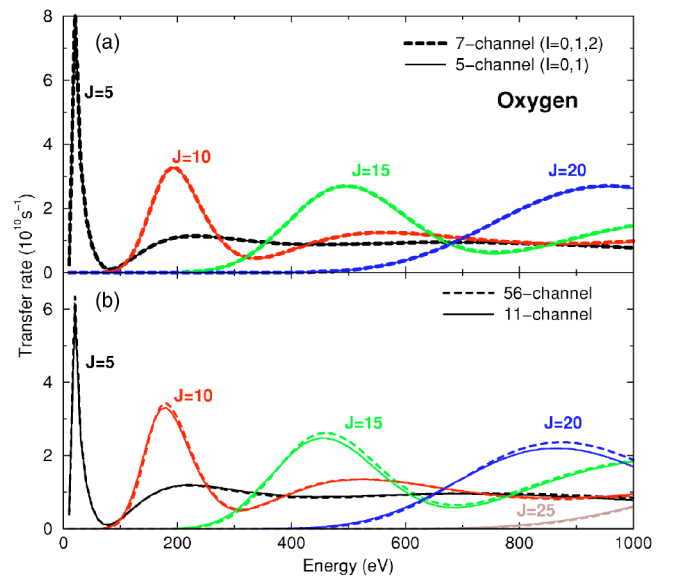


FIG. 9. (Color online) High-energy convergence test for  $p\mu(1s)\text{-O}^{8+}$ .

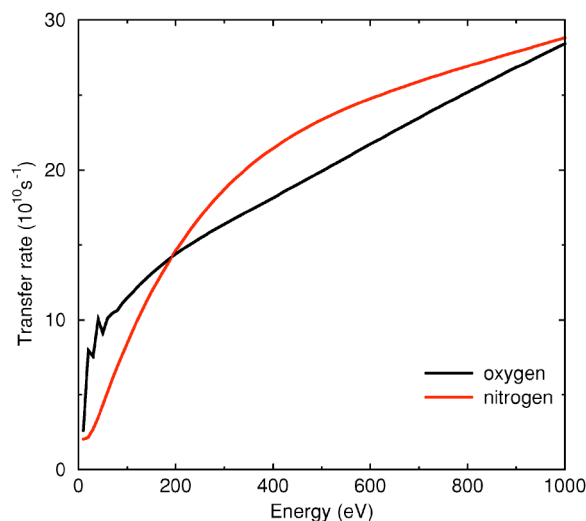


FIG. 10. (Color online) Total muon-transfer rate for  $p\mu(1s)$  colliding with oxygen and nitrogen at collision energies below 1 keV.

#### IV. SUMMARY AND CONCLUSIONS

We have presented the results of diabatic hyperspherical close-coupling calculations for muon transfer in muonic hydrogen colliding with atomic oxygen and nitrogen for the energy range from 1 meV up to 1 keV. The calculated muon-transfer rate for nitrogen was in very good agreement with experiments. However, discrepancies with experiments as well as with earlier calculations were found for oxygen with the “bare” nuclear charge  $O^{8+}$ , where our muon-transfer rate is about a factor of 3 higher than the other results. The large

$p$ -wave resonance was found to be responsible for that dramatic increase in the rate at thermal energies. However, with the screening effect taken into account by a simple Thomas-Fermi potential, the calculated value for the rate decreased by a factor of 5, implying the importance of the screening due to the atomic electrons at thermal energies. It is possible that a more elaborate account of the realistic interaction between oxygen and muonic hydrogen can reproduce the thermal rate extracted from the experimental data and perhaps even the large epithermal rate found by Monte Carlo simulations. The origin of the discrepancy between our results and those of Dupays *et al.* [12] and Dupays [13] for the unscreened interaction is not known.

The results of this paper clearly show that by using the diabatic basis set combined with the elimination of weak channels, one can obtain converged cross sections with a much smaller number of channels in the close-coupling calculations, compared to the traditional adiabatic approach. This is of importance especially for the cases where large numbers of channels are involved. The highly excited Rydberg states especially near the three-body breakup threshold can serve as an example of these systems.

#### ACKNOWLEDGMENTS

This work was supported in part by the Chemical Sciences, Geosciences and Biosciences Division, Office of Basic Energy Sciences, Office of Science, U.S. Department of Energy. We thank Dr. X.-M. Tong for discussions on the screening effect and for providing us with his screening potential.

- 
- [1] L. I. Ponomarev, *Hyperfine Interact.* **138** 15 (2001).
  - [2] L. Schellenberg, *Muon Catal. Fusion* **5/6**, 73 (1990/1991).
  - [3] R. Jacot-Guillarmod, F. Mulhauser, C. Piller, and H. Schneuwly, *Phys. Rev. Lett.* **65**, 709 (1990).
  - [4] R. Jacot-Guillarmod, *Phys. Rev. A* **51**, 2179 (1995).
  - [5] A. Werthmüller *et al.*, *Hyperfine Interact.* **116**, 1 (1998).
  - [6] D. Bakalov, E. Milotti, C. Rizzo, A. Vacchi, and E. Zavattini, *Phys. Lett. A* **172**, 277 (1993).
  - [7] D. Taqqu *et al.*, *Hyperfine Interact.* **119**, 311 (1999).
  - [8] A. Adamczak, D. Bakalov, K. Bakalova, E. Polacco, and C. Rizzo, *Hyperfine Interact.* **136**, 1 (2001).
  - [9] S. S. Gershtein, *Sov. Phys. JETP* **16**, 501 (1963).
  - [10] R. A. Sultanov and S. K. Adhikari, *Phys. Rev. A* **62**, 022509 (2000).
  - [11] A. Dupays, B. Lepetit, J. A. Beswick, C. Rizzo, and D. Bakalov, *Phys. Rev. A* **68**, 062506 (2003).
  - [12] A. Dupays, B. Lepetit, J. A. Beswick, C. Rizzo, and D. Bakalov, *Phys. Rev. A* **69**, 062501 (2004).
  - [13] A. Dupays, *Phys. Rev. Lett.* **93**, 043401 (2004).
  - [14] A. V. Kravtsov, A. I. Mikhailov, and N. P. Popov, *J. Phys. B* **19**, 2579 (1986).
  - [15] A. Kravtsov, A. Mikhailov, and N. Popov, *Phys. Lett. A* **223**, 129 (1996).
  - [16] V. I. Savichev and R. Blümel, *Eur. Phys. J. D* **21**, 3 (2002).
  - [17] S. V. Romanov, *Eur. Phys. J. D* **28**, 11 (2004).
  - [18] M. Hesse, A. T. Le, and C. D. Lin, *Phys. Rev. A* **69**, 052712 (2004).
  - [19] A. T. Le, C. D. Lin, L. F. Errea, L. Mendez, A. Riera, and B. Pons, *Phys. Rev. A* **69**, 062703 (2004).
  - [20] T. G. Lee, M. Hesse, A. T. Le, and C. D. Lin, *Phys. Rev. A* **70**, 012702 (2004).
  - [21] C. N. Liu, A. T. Le, T. Morishita, B. D. Esry, and C. D. Lin, *Phys. Rev. A* **67**, 052705 (2003).
  - [22] A. T. Le, M. W. J. Bromley, and C. D. Lin, *Phys. Rev. A* (to be published).
  - [23] J. C. Light and R. B. Walker, *J. Chem. Phys.* **65**, 4272 (1976).
  - [24] O. I. Tolstikhin, S. Watanabe, and M. Matsuzawa, *J. Phys. B* **29**, L389 (1996).
  - [25] L. D. Landau and E. M. Lifshitz, *Quantum Mechanics* (Pergamon, Oxford, 1965).
  - [26] H. R. Sadeghpour *et al.*, *J. Phys. B* **33**, R93 (2000).
  - [27] A. F. Starace and G. L. Webster, *Phys. Rev. A* **19**, 1629 (1979).
  - [28] H. Schneuwly, *Phys. Lett. A* **191**, 416 (1994).